Supplemental Materials

One-Step Etching-Functionalization of MXene with Preserved Structural Integrity for Ultrahigh Uranium Extraction

Dawang Li, Yan Liu*, Zhirong Liu, Changfu Wang, Yun Wang, Ruiming Zhang, Hao Jiang*

National Key Laboratory of Uranium Resources Exploration-Mining and Nuclear Remote Sensing, East China University of Technology, Nanchang, Jiangxi 330013, PR China

* Corresponding author: E-mail: fzliuyan1986@163.com; jianghao@ecut.edu.cn

Experimental section

Materials

Uranyl nitrate hexahydrate ($UO_2(NO_3)_2·6H_2O$, AR) was obtained from Hubei Chushengwei Chemical Co., Ltd. Ti_3AlC_2 was acquired from Xinxi Technology Co., Ltd. Hydrochloric acid (HCl, 38%), nitric acid (HNO_3, 98%), and trifluoromethanesulfonic acid (CF_3SO_3H, AR) were supplied from Xilong Scientific Co., Ltd. All chemicals were of analytical grade and used as received without further purification.

Synthesis of the TCS membrane

In a typical procedure, 1.0 g of Ti_3AlC_2 MAX phase precursor was added to a premixed etching solution containing 15 mL of CF_3SO_3H and 5 mL of deionized water under N_2. The etching reaction proceeded for 24 h at 40 °C in an oil bath with continuous mechanical stirring at 300 rpm to selectively remove the Al layers. The resulting mixture was washed with 2 M HCl via centrifugation at 5000 rpm to remove residual etchant and AlF_3 by-products, followed by repeated centrifugation with deionized water until the supernatant reached a neutral pH of approximately 6. The collected sediment was dispersed in an ice-water bath and ultrasonicated for 1 h to facilitate delamination. After centrifugation at 3500 rpm for 15 min to remove unexfoliated particles, the supernatant colloidal suspension was collected and diluted to a concentration of 5 mg/mL. Finally, 6 mL of this suspension was mixed with 6 mL

of deionized water, and dried under vacuum at 60 °C to yield the self-supporting TCS membrane with a loading area of 1 mg/cm².

Characterization

Fourier transform infrared spectroscopy (FTIR, TENSOR27) was utilized to investigate the functional groups of the samples. Morphological and elemental distribution analysis were conducted by scanning electron microscopy (SEM, JEOL JSM-5900) coupled with energy dispersive X-ray spectroscopy (EDS). Chemical states and surface compositions were determined by X-ray photoelectron spectroscopy (XPS, Kratos Axis Ultra DLD). Crystalline phases were carried out using X-ray Diffraction (XRD, D8 Advance) with Cu Kα radiation. Specific surface area and pore size distribution were identified by nitrogen adsorption-desorption isotherms measured on a V-Sorb 2800TP analyzer. All electrochemical performance was carried out on a CHI660E electrochemical workstation (CH Instruments, shanghai).

Batch adsorption experiments

Batch adsorption experiments were conducted at 298 K under various conditions, including different pH values, mass ratios, contact time and initial U(VI) concentrations. The pH value of U(VI) solution was regulated by 0.1 mol/L HCl and 0.1 mol/L NaOH. The concentration of U(VI) before and after adsorption was determined by the arsenazo(III) method. The adsorption capacity q_t (mg/g) was calculated based on the following equation:

$$q_t = (C_0 - C_e)V/m \tag{S1}$$

where C_0 and C_e (mg/L) represents the initial and equilibrium concentrations of (VI), respectively; V (L) stands for the volume of the solution and m (g) is the mass of the adsorbent.

Adsorption kinetics and isotherm models

Pseudo-first-order and Pseudo-second-order were employed to evaluate the adsorption process. The nonlinear forms of the two models are given by:

Pseudo-first-order:

$$q_t = q_e(1 - e^{-k_1 t}) \tag{S2}$$

Pseudo-second-order:

$$q_t = \frac{k_2 q_e^2 t}{1 + k_2 q_e t} \tag{S3}$$

Where q_e (mg/g) and q_t (mg/g) are the equilibrium adsorption capacity and adsorption capacity at t (min), respectively; k_1 (min^{-1}) and k_2 ($g \cdot mg^{-1} \cdot min^{-1}$) represent the rate constants for pseudo-first-order and pseudo-second-order, respectively.

The equilibrium adsorption data were fitted with the Langmuir and Freundlich isotherm models, depicted as:

Langmuir:

$$q_e = \frac{q_m K_L C_e}{1 + K_L C_e} \tag{S4}$$

Freundlich:

$$q_e = K_F C_e^{1/n} \tag{S5}$$

Where C_e (mg/L) is the equilibrium concentration of U(VI); q_m (mg/g) and K_L (L/mg) are the theoretical maximum adsorption capacity and the Langmuir constant related to adsorption energy, respectively; n and K_F (mg/g) are the Freundlich constants indicative of adsorption capacity and intensity, respectively.

Electrochemical tests

Electrochemical impedance spectroscopy (EIS) was performed using a standard three-electrode system with a platinum counter electrode and a Hg/Hg_2Cl_2 reference electrode (saturated KCl, isolated by a double salt bridge to minimize Cl^- leakage). The electrolyte was 1 M H_2SO_4. The frequency range was 0.01 Hz to 10^5 Hz. Linear sweep voltammetry (LSV) was conducted with a platinum counter electrode and an Ag/AgCl reference electrode (3 M KCl) in an electrolyte containing 200 ppm U(VI) and 0.5 M Na_2SO_4 at a scan rate of 0.2 mV/s. The different reference electrodes were chosen based on specific requirements: Hg/Hg_2Cl_2 provides superior potential stability and minimal Cl^- leakage for impedance measurements, whereas Ag/AgCl offers lower liquid junction impedance for sensitive voltammetry in sulfate-rich solutions where any minor Cl^- leakage is negligible. The low scan rate of 0.2 mV/s was chosen to allow the system to approach thermodynamic equilibrium, suppress charging current interference, and resolve the multi-step reduction pathways (U(VI)→U(V)→U(IV)). The 0.5 M Na_2SO_4 electrolyte is near-neutral, which is critical for studying U(VI) reduction, and its concentration provides adequate ionic strength to control solution interactions.

Electrochemical Uranium Adsorption

Electrochemical uranium extraction experiments were performed in a two-electrode system using a platinum as the anode and the TCS membrane as the cathode.

A square-wave voltage was applied using a function/arbitrary waveform generator (DG1022Z), with a voltage range of 0 to -5 V and a frequency of 400 Hz. All experiments were replicated three times.

Energy consumption calculation model

$E_{total}=\int_{0}^{t_{total}} V(t)\, I(t)dt$

Where total represents the total extraction time, V(t) denotes the applied square wave potential, and I(t) signifies the measured response current

Energy consumption per unit mass:

$W= E_{total}/mU$ ($kWh\cdot kg^{-1}$)

Electrode elution experiment

The electrode was immersed in 20 mL of 0.1M HNO_3 desorption agent with shaking at room temperature for 30 minutes. Then the electrode is thoroughly rinsed with deionized water 2–3 times.

Computational details

All density functional theory (DFT) calculations were carried out using the CP2K code[1]. All calculations utilized a hybrid Gaussian and plane wave basis set. Core electrons were modeled using norm-conserving Goedecker-Teter-Hutter pseudopotentials[2–4], while the valence electron wavefunction was extended in a double-zeta basis set with polarization functions[5], supplemented with an auxiliary plane wave basis set with an energy cutoff of 450 Ry. The generalized gradient approximation exchange-correlation functional of Perdew, Burke, and Enzerhof (PBE)[6] was used. Each configuration was optimized using the Broyden-Fletcher-Goldfarb-Shanno (BFGS) method with a self-consistent field (SCF) convergence criterion of 1.0×10^{-5} au. To account for the long-range van der Waals dispersion interaction, the DFT-D3 scheme[7], incorporating an empirical damped potential factor, was integrated into the energies derived from the exchange-correlation functional in all calculations. The interaction energy between the adsorbate and the substrate can be determined using the subsequent equation:

$$\Delta E_{ads} = E_{(adsorbate@substrate)} - E_{substrate} - E_{adsorbate} \quad (S6)$$

where $E_{(adsorbate@substrate)}$ and $E_{substrate}$ represent the total energies of the substrate with and without the adsorbate, respectively. $E_{adsorbate}$ is the total energy of the

adsorbate UO_2^{2+}. According to this equation, a negative ΔE_{ads} indicates a thermodynamically stable adsorption configuration.

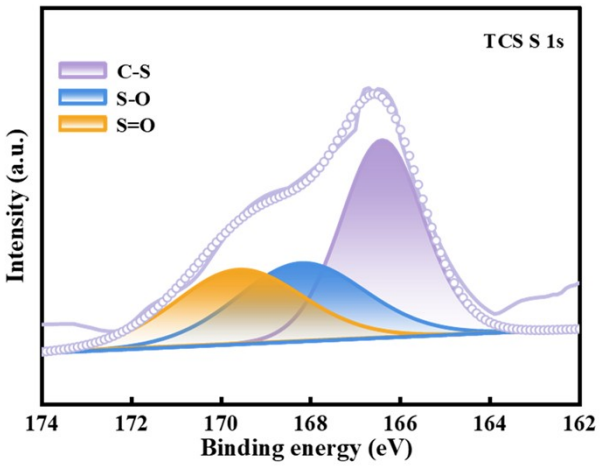

Fig. S1 S 1s regions of TCS.

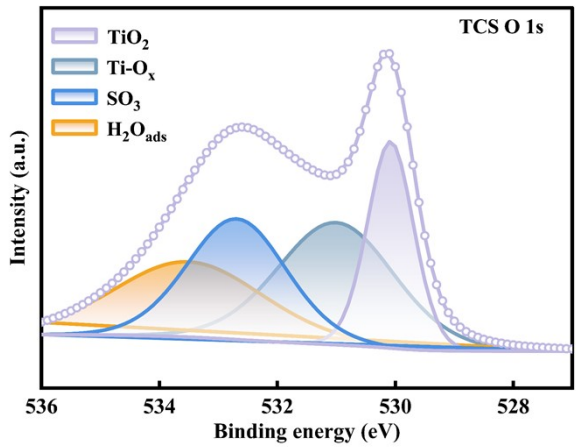

Fig. S2 O1s regions of TCS.

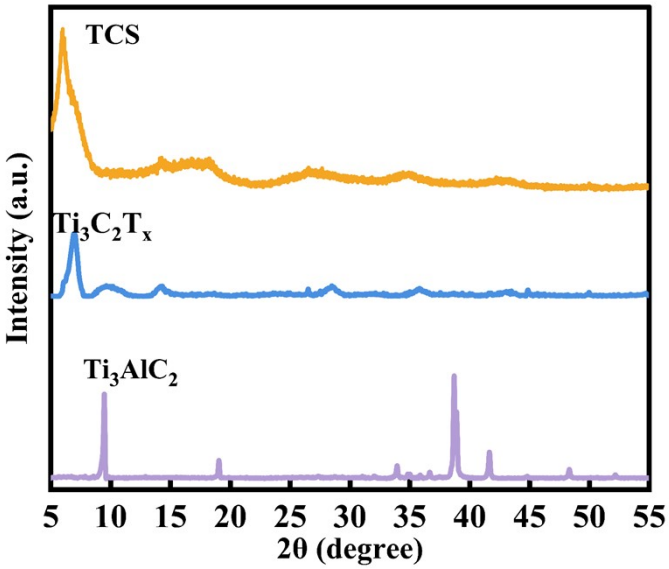

Fig. S3 XRD patterns of $Ti_3C_2T_x$ and TCS.

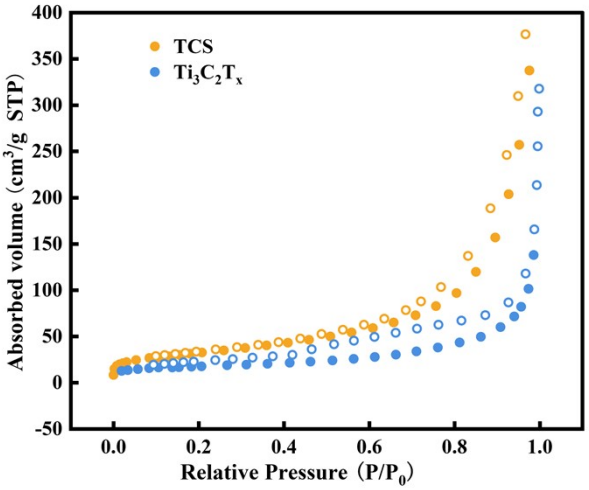

Fig. S4 N_2 adsorption-desorption isotherms of $Ti_3C_2T_x$ and TCS.

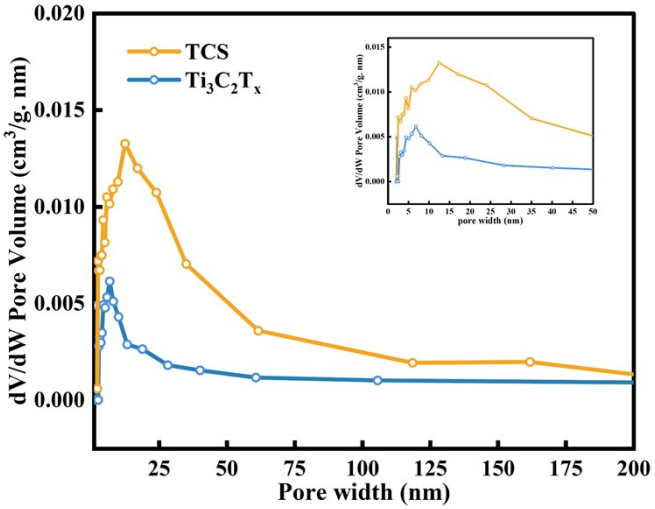

Fig. S5 Pore size distribution curves of $Ti_3C_2T_x$ and TCS.

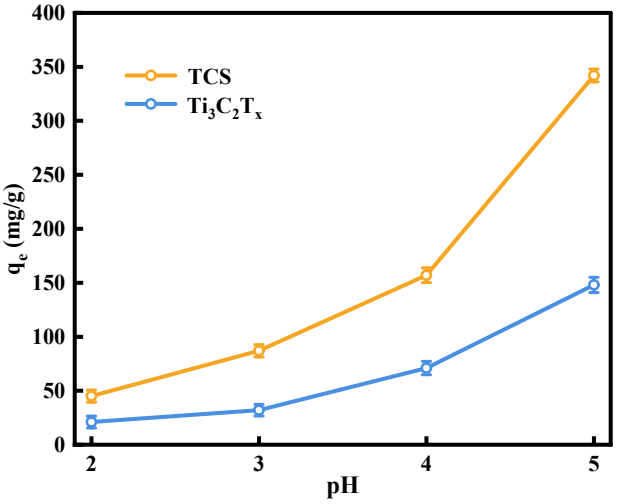

Fig. S6 The influence of different pH on the adsorption capacity of U(VI) (t=180 min).

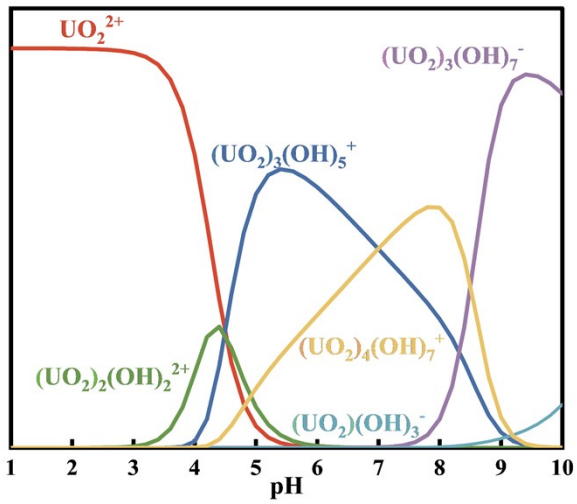

Fig. S7 Uranium morphology at different pH values.

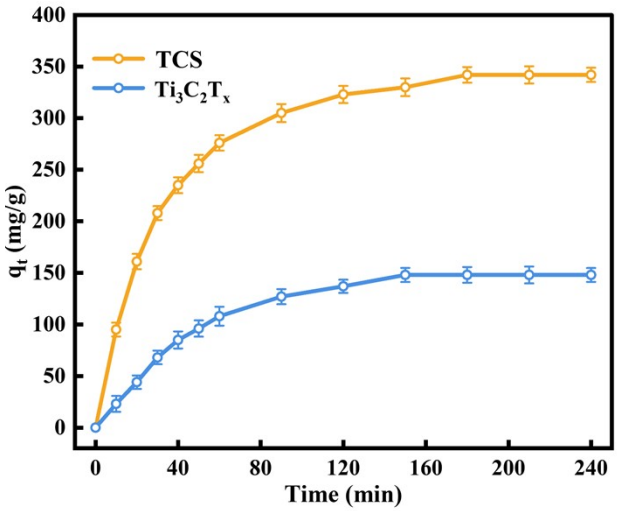

Fig. S8 Effect of time on adsorption performance (v/m=5, t=180 min, pH=5).

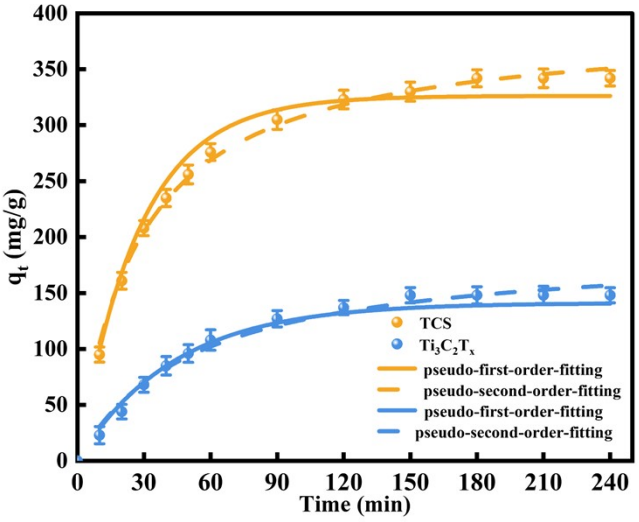

Fig. S9 Adsorption fitting kinetics for U(VI) adsorption of $Ti_3C_2T_x$ and TCS.

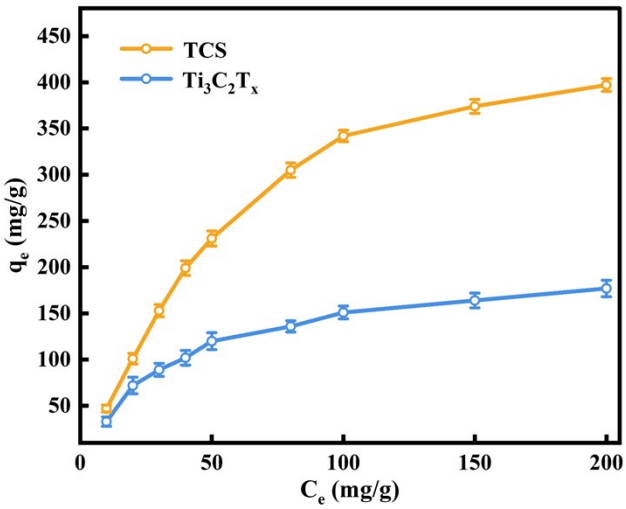

Fig. S10 Effect of initial concentration (v/m=5, t=180 min) on the adsorption capacity of U(VI).

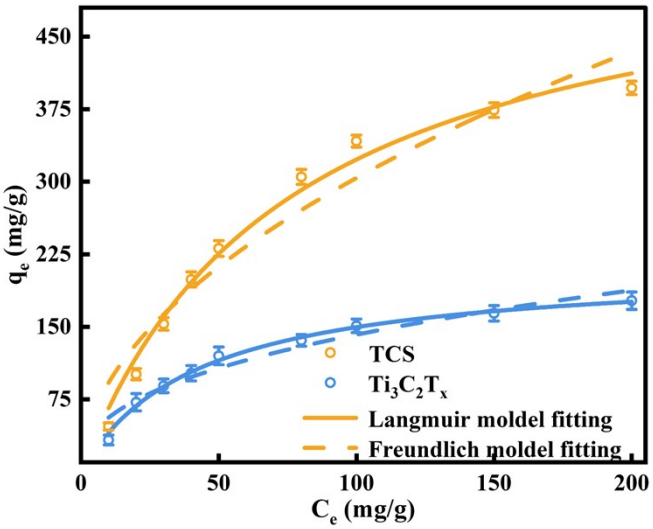

Fig. S11 Adsorption isotherms of $Ti_3C_2T_x$ and TCS.

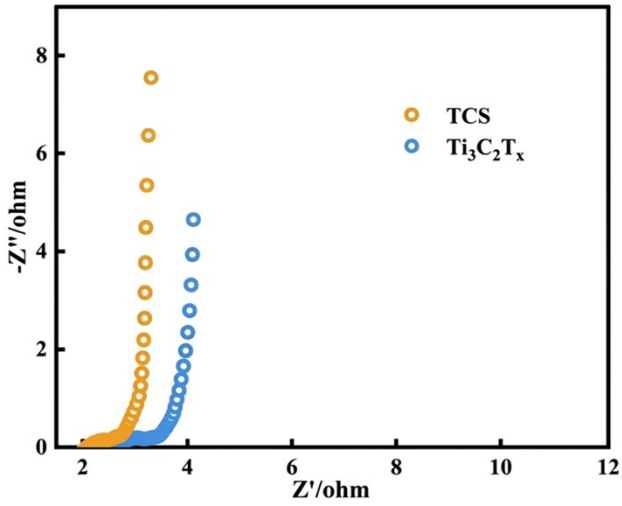

Fig. S12 EIS spectra of $Ti_3C_2T_x$ and TCS.

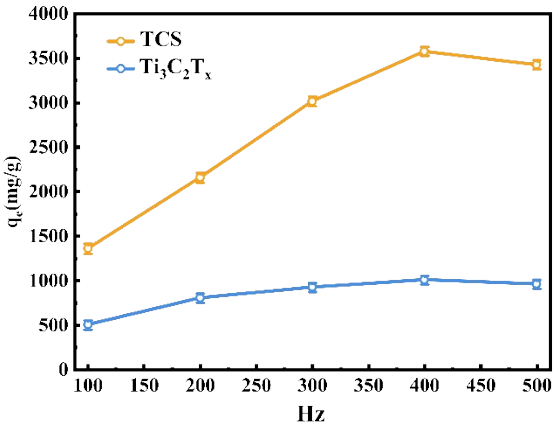

Fig S13 Effect of frequency on electro-extraction performance of U(VI) (pH=5, C_0=200 ppm, v/m=20).

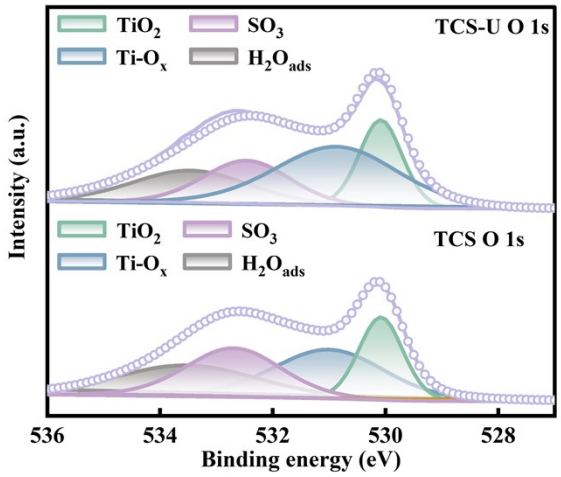

Fig. S14 O 1s regions of TCS and TCS-U.

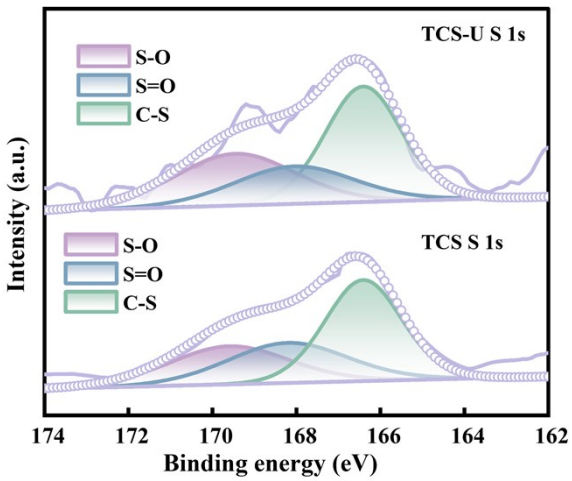

Fig. S15 S 1s region of TCS and TCS-U.

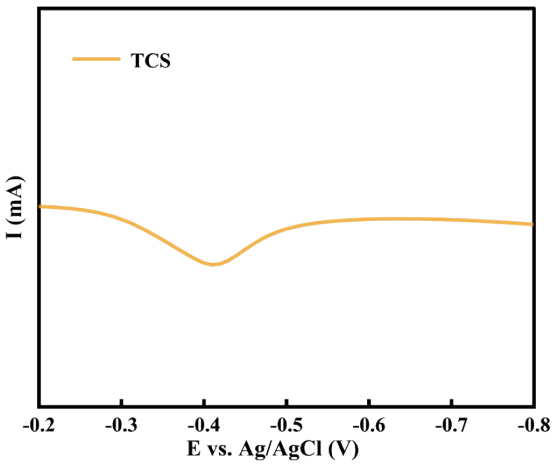

Fig. S16 LSV curve of TCS under uranium-spiked water.

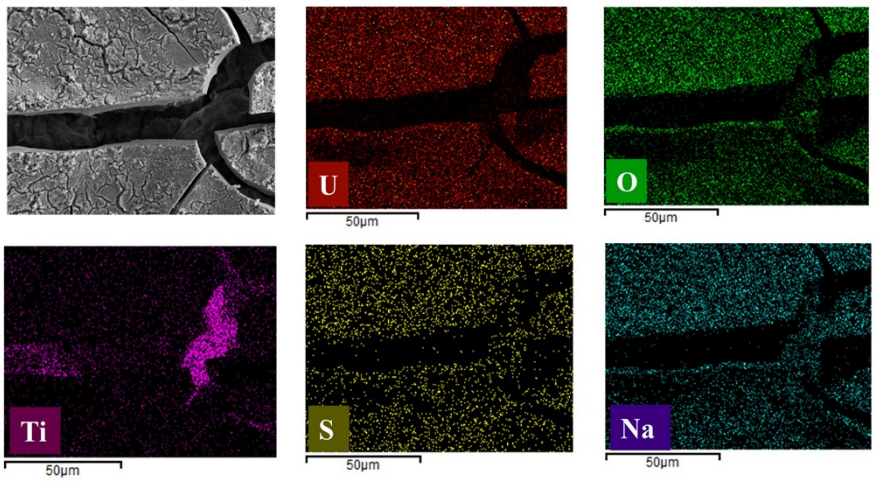

Fig. S17 SEM image of TCS after electrochemical uranium extraction experiment and EDS spectra of the corresponding elements.

Table S1 Kinetic parameters for the pseudo-first-order and pseudo-second-order kinetic models onto $Ti_3C_2T_x$ and TCS membrane.

Sample	$q_{e,exp}$ (mg/g)	Pseudo-first-order model			Pseudo-second-order model		
		$q_{1,cal}$ (mg/g)	k_1 (min^{-1})	R^2	$q_{2,cal}$ (mg/g)	k_2 (min^{-1})	R^2
$Ti_3C_2T_x$	148.64	141.19	2.2×10^{-2}	0.9771	190.91	1.03×10^{-4}	0.9816
TCS	324.51	310.14	3.6×10^{-2}	0.9790	381.65	1.36×10^{-4}	0.9993

Table S2 Langmuir and Freundlich isothermal adsorption fitting parameters of $Ti_3C_2T_x$ and TCS.

Sample	Langmuir			Freundlich		
	q_m(mg/g)	K_L(L/mg)	R^2	K_F(□ (mg/g)(L/mg)$^{1/n}$)	n	R^2
$Ti_3C_2T_x$	213.31	2.3×10^{-2}	0.9933	22.17	2.48	0.9735
TCS	568.95	1.3×10^{-2}	0.9874	27.98	1.93	0.9379

Table S3 Comprehensive comparison of various electrode materials with TCS.

Material	Material Type	Ligands	Self-supporting	Operation Mode	Extraction Capacity(mg/g)	Capacity retention after five cycles (%)	Uranium Product Form
TCS	MXene	$-CF_3SO_3$	Yes	SWE	3576.3	93	$Na_2U_2O_7$
PPy@$MoSe_2$@MXene[8]	MXene	PPy + $MoSe_2$	No	CDI	659	84	UO_2
MMA[9]	MXene / MOF	AO	No	FCDI	2322.4	90.5	UO_2
TAZ[10]	MXene / MOF	AO + ZIF-67	No	Electrosorption	2224.54	63.51	UO_2
CP@C[11]	COF	AO	Yes	HW-ACE)	3838	94	$Na_2O(UO_3{\cdot}H_2O)_x$
PyHATP[12]	polymer	C=O/C=N	No	CDI	600–800	93	UO_2

References

1 S. Grimme, J. Antony, S. Ehrlich and H. Krieg, *The Comput. Phys. Commun*, 2010, **132**, 154104.

2 J. VandeVondele and J. Hutter, *J. Chem. Phys.*, 2007, **127**, 114105.

3 C. Hartwigsen, S. Goedecker, J. Hutter, *Phys. Rev. B* 1998, **58**, 3641-36624

4 J. VandeVondele, M. Krack, F. Mohamed, M. Parrinello, T. Chasseing and J. Hutter, *Phys. Chem. Chem. Phys.*, 2005, **167**, 103–128.

5 J. VandeVondele, J. Hutter, *J. Chem. Phys.* 2007, **127**, 114105.

6 J. Perdew, K. Burke, M. Ernzerhof, *Phys. Rev. Lett.* 1996, **77**, 3865.

7 S. Grimme, J. Antony, S. Ehrlich, H. Krieg, *J. Chem. Phys.* 2010, **132**, 154104.

8 X. L. Cai, X. Yao, L. Zhang, Y. H. Chai, X. Liu, W. W. Liu, R. X. Zhang, Y. Y. Fan and X. Xiao, *J. Hazard. Mater.*, 2024, **480**, 136371.

9 Y. Wang, Z. Lu, M. Luo, Z. Zhao, Y. Wei and H. Wang, *Sep. Purif. Technol.*, 2024, **335**, 126134.

10 N. Li, L. Yang, R. Su, N. Shi, J. Wu, J. Zhao, L. Wen and Z. Wang, *Desalination*, 2023, **566**, 116940.
11 S. Wang, P. Zhang, Z. Wang, J. Wang, C. Jiang, J. Yu and S. Chen, *Sep. Purif. Technol.*, 2026, **380**, 135220.
12 S. Ma, Z. Han, X. Bai, J. Kong and G. Ran, *Coord. Chem. Rev.*, 2026, **549**, 217248.